Superior Optical Properties of Perovskite Nanocrystals as Single Photon Emitters

Fengrui Hu,[†,⊥] Huichao Zhang,[†,§,⊥] Chun Sun,[‡] Chunyang Yin,[†] Bihu Lv,[†] Chunfeng Zhang,[†] William W. Yu,[‡] Xiaoyong Wang,[*,†] Yu Zhang,[*,‡] and Min Xiao[*,†,∥]

[†]National Laboratory of Solid State Microstructures, School of Physics, and Collaborative Innovation Center of Advanced Microstructures, Nanjing University, Nanjing 210093, China, [‡]State Key Laboratory on Integrated Optoelectronics and College of Electronic Science and Engineering, Jilin University, Changchun 130012, China, [§]College of Electronics and Information, Hangzhou Dianzi University, Xiasha Campus, Hangzhou 310018, China, and [∥]Department of Physics, University of Arkansas, Fayetteville, Arkansas 72701, United States. [⊥]F. Hu and H. Zhang contributed equally to this work.

ABSTRACT The power conversion efficiency of photovoltaic devices based on semiconductor perovskites has reached ~20% after just several years of research efforts. With concomitant discoveries of other promising applications in lasers, light-emitting diodes, and photodetectors, it is natural to anticipate what further excitement these exotic perovskites could bring about. Here we report on the observation of single photon emission from single $CsPbBr_3$ perovskite nanocrystals (NCs) synthesized from a facile colloidal approach. Compared with traditional metal-chalcogenide NCs, these $CsPbBr_3$ NCs exhibit nearly 2 orders of magnitude increase in their absorption cross sections at similar emission colors. Moreover, the radiative lifetime of $CsPbBr_3$ NCs is greatly shortened at both room and cryogenic temperatures to favor an extremely fast output of single photons. The above superior optical properties have paved the way toward quantum-light applications of perovskite NCs in various quantum information processing schemes.

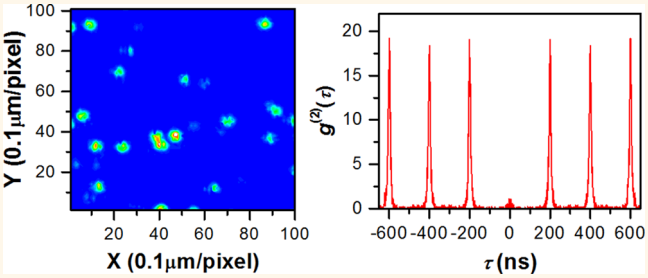

KEYWORDS: perovskite · nanocrystal · single photon emission · blinking

Single optical emitters such as natural atoms[1] and molecules[2] are able to emit single photons due to the time interval needed for the electron to recycle between the two-level ground and excited states. This kind of quantum-light emission has been intensively pursued and manipulated since it can provide a robust platform to test fundamental quantum-optical and measurement theories as well as to promote practical quantum information processing applications in terms of quantum computing, teleportation, and cryptography.[3,4] So far, single photon emission has been discovered in a very limited number of artificially engineered fluorescent materials ranging from epitaxial quantum dots (QDs),[5] colloidal nanocrystals (NCs),[6] and diamond color centers[7] to carbon nanotubes[8] and most recently to Pr^{3+}:YAG crystals,[9] 4H-SiC wafers,[10] and atomically thin layers of 2D WSe_2.[11] Most of the above single photon sources are associated with structural/compositional defects whose exact origins are sometimes illusive, while only epitaxial QDs and colloidal NCs can be predictably and reproducibly produced with size- and shape-dependent optical properties dictated by the quantum confinement effect. When the selection criterion for single photon sources is raised even higher to be more relevant to practical applications, colloidal NCs are eventually singled out as the unique candidate capable of emitting visible light at room temperature. After nearly two decades of intensive research, a rich spectrum of optical phenomena has been revealed from colloidal NCs at the single-particle level,[12] the understanding of which is continuously promoting their potential applications such as in biotechnology, medicine, electronics, and optoelectronics.[13] One open question of immediate importance is whether a brand new class of colloidal NCs, other than the current ones based almost solely on metal chalcogenides (*e.g.*, CdSe NCs), can be

* Address correspondence to
(X. Wang) wxiaoyong@nju.edu.cn;
(Y. Zhang) yuzhang@jlu.edu.cn;
(M. Xiao) mxiao@uark.edu.

Received for review September 13, 2015 and accepted October 31, 2015.

Published online
10.1021/acsnano.5b05769

judiciously synthesized to demonstrate their structure- and composition-specific single photon emitting properties.

Semiconductor perovskites can be conveniently described by the formula ABX_3 with A, B, and X being an organic or inorganic cation, a metal cation, and a halide anion, respectively. Within just the last several years, the power conversion efficiency of solar cells incorporating perovskites as light harvesters has been dramatically increased from the original ~3.8% to the current value of ~20%.[14−20] This stunning performance of perovskites in solar cells benefits largely from their easy solution processing, suitable energy gap, and high absorption coefficient, in addition to the high mobility, long diffusion length, and slow radiative recombination of photoexcited charge carriers. These unique material and optical properties of perovskites can also be applied to several other optoelectronic devices, with their debut appearances in light-emitting diodes,[21] lasers,[22] and photodetectors[23] having been sequentially demonstrated. To bring the remaining potentials of perovskites into full play, it is imperative to obtain a deeper understanding of the underlying photophysics[24,25] and to fabricate larger-sized single crystals with lower densities of structural defects and carrier traps.[26−28] Meanwhile, with several initial attempts to reduce the size of bulk perovskites to the submicrometer scale,[29,30] colloidal NCs of both cesium and methylammonium lead halides have been recently synthesized.[31−33] These achievements not only provide a flexible tunability for the size-dependent fluorescent colors of perovskites but also prepare a necessary condition to explore their quantum-light nature of single photon emissions.

Here we focus on optical characterizations of single $CsPbBr_3$ (cesium lead bromide) perovskite NCs whose sizes are close to the exciton Bohr diameter to reach the quantum-confined regime. At room temperature, the photoluminescence (PL) intensity of single $CsPbBr_3$ NCs switched between the "on" and "off" periods intermittently (also called blinking), which can be attributed to random formation of charged excitons and the associated nonradiative Auger recombination. The same Auger process also greatly suppressed the radiative recombination of multiexcitons, leading to almost complete single photon emissions from single $CsPbBr_3$ NCs. At cryogenic temperature, the PL line width of a single NC was as broad as ~1 meV under the influence of the spectral diffusion effect. While the above optical behaviors are on par with those observed in conventional metal-chalcogenide NCs, these $CsPbBr_3$ NCs have exhibited a nearly 2 orders of magnitude increase in their absorption cross sections. Moreover, the PL lifetime of single NCs is greatly shortened at both room and cryogenic temperatures to favor an extremely fast output of single photons.

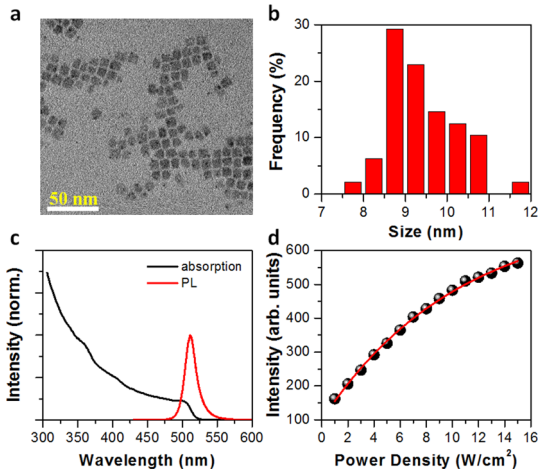

Figure 1. (a) Transmission electron microscopy of $CsPbBr_3$ NCs. (b) Histogram for the size distribution of $CsPbBr_3$ NCs. (c) Solution absorption and emission spectra measured for ensemble $CsPbBr_3$ NCs. (d) PL intensity of ensemble $CsPbBr_3$ NCs measured as a function of the laser power density P and fitted with the function $\propto 1 - e^{-\alpha P}$, where α is a fitting constant related to the absorption cross section.

RESULTS AND DISCUSSION

According to a previous report,[32] perovskite $CsPbBr_3$ NCs used in the current experiment were synthesized from a colloidal approach (see Experimental Section) with a cubic shape and an average size of ~9.4 nm, as estimated from the transmission electron microscopy measurement (Figure 1a,b). The NC dimension is close to the Bohr diameter of ~7 nm estimated for the Wannier−Mott excitons of $CsPbBr_3$ perovskites,[32] so that the quantum confinement effect can be expected. The first absorption band and the PL peak measured from ensemble $CsPbBr_3$ NCs are located at ~504 nm (~2.46 eV) and ~511 nm (~2.43 eV), respectively (Figure 1c), corresponding to an energy gap that is blue-shifted by ~200 meV relative to the bulk value of ~2.25 eV.[34] With pulsed laser excitation at 405 nm, we measured the PL intensity of ensemble $CsPbBr_3$ NCs as a function of the laser power density (Figure 1d). For bulk perovskite films, the PL intensity increases almost continuously with the increasing laser power density,[35] which is usually accompanied by a blue shift and an obvious broadening of the PL spectrum due to the band-filling effect.[24] Then the PL saturation effect (Figure 1d) and the invariant PL line shape (see Supporting Information, Figure S1) measured for ensemble $CsPbBr_3$ NCs with increasing laser power densities are strong evidence that optical emissions originate from atomic-like, discrete energy levels.[7−9]

With the excitation of the same 405 nm pulsed laser, we further performed optical characterizations of single $CsPbBr_3$ NCs at room temperature unless otherwise specified in the text (see Experimental Section). In Figure 2a, we plot a confocal scanning PL image acquired from a sample region of 10 μm × 10 μm, where each bright spot corresponds to the optical

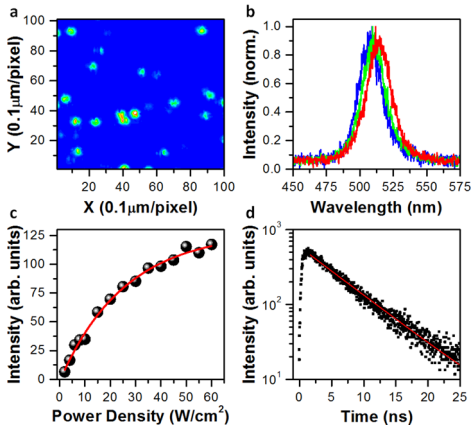

Figure 2. (a) Confocal scanning PL image of single $CsPbBr_3$ NCs. The scanning step was 100 nm, and the dwell time at each pixel is 100 ms. (b) PL spectra of three single $CsPbBr_3$ NCs obtained with an integration time of 10 s. (c) PL intensity of a single $CsPbBr_3$ NC measured as a function of the laser power density P and fitted with the function $\propto 1 - e^{-\alpha P}$, where α is a fitting constant related to the absorption cross section. (d) PL decay curve of a single $CsPbBr_3$ NC fitted by a single-exponential function with a radiative lifetime of ~6.44 ns.

emission from a single $CsPbBr_3$ NC. The PL spectra of three single $CsPbBr_3$ NCs are shown in Figure 2b with an average fwhm (full width at half-maximum) of ~100 meV (~25 nm). Due to the inhomogeneous size distribution (Figure 1a,b), these PL peaks vary in the range ~505−515 nm, which is a clear demonstration of the size-dependent energy gaps of the $CsPbBr_3$ NCs. In Figure 2c, we also plot the PL intensity of a representative single NC as a function of the laser power density, and a similar PL saturation effect to the one shown in Figure 1d for ensemble NCs can be observed. With $\langle N \rangle$ representing the average number of photons absorbed per NC per pulse, the PL saturation curve can be fitted with a functional form $\propto 1 - e^{-\langle N \rangle} = 1 - e^{-j\sigma}$,[36] where σ and j are the absorption cross section of the NC and the pump fluence of the laser, respectively. Since the pump fluence j is a controllable parameter in our experiment, the absorption cross section σ of this single NC can be reliably estimated to be $\sim 1.23 \times 10^{-13}$ cm^2. A similar σ of $\sim 2.33 \times 10^{-13}$ cm^2 can be obtained from the PL saturation curve shown in Figure 1d, which can be treated as the average absorption cross section of ensemble $CsPbBr_3$ NCs at the excitation wavelength of 405 nm. Compared to traditional metal-chalcogenide CdSe NCs emitting at similar wavelengths, the σ value measured here for $CsPbBr_3$ NCs is enhanced by almost 2 orders of magnitude (see Experimental Section), indicating that they have inherited the excellent absorption capacity of bulk perovskites.

For convenience, we next performed all the optical characterizations of single $CsPbBr_3$ NCs at $\langle N \rangle \approx 0.1$ to avoid any nonlinear effect unless otherwise specified in the text. As measured for a representative $CsPbBr_3$ NC, the PL decay curve can be fitted by a single-exponential function with a lifetime constant of ~6.44 ns (Figure 2d), which is a typical value for nearly all the single $CsPbBr_3$ NCs studied in our experiment (see Supporting Information Figure S2 for the PL decay curves of two additional NCs). This radiative lifetime of ~6.44 ns is significantly shorter than the counterpart value of hundreds of nanoseconds normally measured for bulk perovskite films,[25,26,28] possibly due to the forced overlap of electron and hole wave functions within the quantum-confined volume. In comparison, the PL decay curve measured at room temperature for single metal-chalcogenide CdSe NCs can also be fitted by a single-exponential function but with a radiative lifetime of ~20 ns and beyond.[6,37]

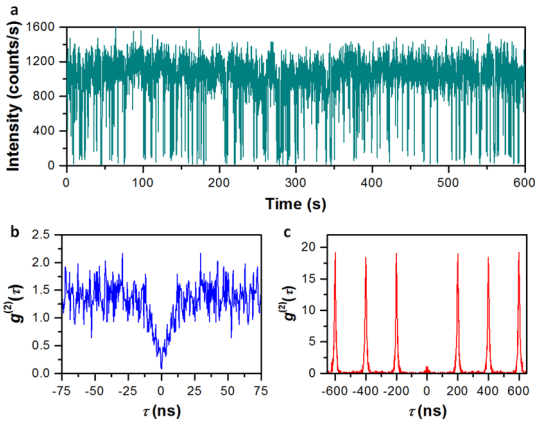

Figure 3. (a) PL time trajectory of a single $CsPbBr_3$ NC with a binning time of 100 ms. (b) Second-order autocorrelation function $g^{(2)}(\tau)$ measurement of a single $CsPbBr_3$ NC under CW excitation. (c) Second-order autocorrelation function $g^{(2)}(\tau)$ measurement of a single $CsPbBr_3$ NC under pulsed excitation.

The PL time trajectory of a representative $CsPbBr_3$ NC is shown in Figure 3a with an obvious PL blinking behavior, which was observed from all the single $CsPbBr_3$ NCs studied in our experiment (see Supporting Information Figure S3 for the PL time trajectories of two additional NCs). The probability densities for the time durations of both blinking "on" and "off" periods roughly follow an inverse power-law distribution with an exponent of ~1.5 (see Supporting Information, Figure S4). Similar to the case of single CdSe NCs,[38] the blinking "off" periods can be attributed to nonradiative Auger recombination of charged excitons formed after the photoexcited electron or hole is captured by an external trap and the subsequent excitation of another electron−hole pair in the single NC. While being negligible in bulk semiconductors, the Auger effect manifests itself strongly in quantum-confined NCs due to the enhanced Coulomb interaction between charge carriers and the alleviated kinematic restriction on momentum conservation.[39] In fact, the existence of Auger interaction between charge

carriers in a single NC is a prerequisite for single photon emission since it provides an efficient channel for nonradiative dissipation of multiexcitons to prevent simultaneous emission of multiple photons.[37] The PL blinking phenomenon recently reported in both $CH_3NH_3PbI_3$ (ref 40) and $CH_3NH_3PbBr_3$ (ref 41) perovskite particles, whose dimensions are much larger than the exciton Bohr diameters, might be caused by some other mechanisms instead of Auger recombination of charged excitons since no single photon emission was observed at the single-particle level.

Single photon emissions were observed in all the single $CsPbBr_3$ NCs studied in our experiment from the second-order autocorrelation function $g^{(2)}(\tau)$ measurements. With the continuous wave (CW) excitation from a 400 nm laser, the ratio between $g^{(2)}(0)$ and $g^{(2)}(\tau)$ at long time delays was calculated to be ~0.06 for a representative NC (Figure 3b). With the pulsed excitation from the 405 nm laser, the average area ratio between the central $g^{(2)}(0)$ and the side $g^{(2)}(nT)$ peaks was calculated to be ~0.06 for another representative NC (Figure 3c), where $n \geq 1$ is an integer and T is the laser repetition time. These excellent photon antibunching features strongly confirm that single $CsPbBr_3$ NCs can serve perfectly as a single photon source. In our experiment, we also increased the laser power density to set $\langle N \rangle$ larger than ~1.0 so that the possibility for the generation of multiexcitons in a single NC should be greatly increased.[37,39] As can be seen in Supporting Information Figure S5 for the pulsed excitation of a representative NC, there was almost no increase in the average area ratio between the central and the side peaks with the increasing laser power density. This implies that Auger recombination of multiexcitons is extremely efficient in single $CsPbBr_3$ NCs, thus rendering a pure single photon stream without random interruptions of multiphoton events.

We have also performed optical characterizations of $CsPbBr_3$ NCs at the cryogenic temperature of ~4 K. Consistent with what was reported previously for bulk $CH_3NH_3PbI_3$ perovskites,[35] the PL peak measured at ~4 K for ensemble $CsPbBr_3$ NCs showed no blue shift when compared to the one measured at room temperature (see Supporting Information, Figure S6). In Figure 4a, we plot the PL spectra of four single $CsPbBr_3$ NCs with the calculated FWHMs that are all slightly smaller than 1 meV. These relatively broad PL spectra reflect the fact that spectral diffusion is still drastic at ~4 K, as can be seen from the time-dependent PL spectral image shown in Figure 4b for two single $CsPbBr_3$ NCs. The PL decay curve of a representative $CsPbBr_3$ NC is shown in Figure 4c, which can be fitted well only by a biexponential function with a fast and a slow lifetime component of ~355 ps and ~5.75 ns, respectively (see Supporting Information Figure S7 for the PL decay curves of two additional $CsPbBr_3$ NCs). For single CdSe NCs, the PL decay also

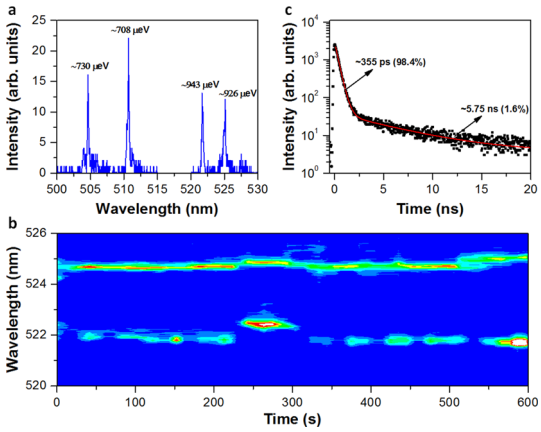

Figure 4. (a) PL spectra of four single $CsPbBr_3$ NCs obtained with an integration time of 10 s. The associated fwhm of each PL spectrum is also shown. (b) Time-dependent PL spectral image for two single $CsPbBr_3$ NCs where the PL blinking and spectral diffusion effects can be clearly observed. The integration time for each PL data point is 10 s. (c) PL decay curve of a single $CsPbBr_3$ NC fitted by a biexponential function with a fast and a slow lifetime of ~355 ps (~98.4%) and ~5.75 ns (~1.6%), respectively.

becomes biexponential at cryogenic temperatures due to electronically coupled optical emissions from a bright state and a lower-lying dark state with a radiative lifetime of hundreds of nanoseconds.[42] The energy-level splitting between the above two states can reach the scale of several millielectronvolts, so that the long-lived dark state cannot be easily depopulated by the thermal energy at cryogenic temperatures, leading to its dominant contribution to the total optical emissions over the bright state in CdSe NCs. If thermal mixing of bright and dark states can really be invoked to explain the PL dynamics observed here for single $CsPbBr_3$ NCs, their energy-level splitting must be significantly smaller than that in CdSe NCs since the slow lifetime component of ~5.75 ns accounts for at most ~5% of the total PL decay.

On the basis of all the experimental results obtained so far, we would like to point out several superior optical properties of the newly synthesized perovskite NCs over traditional metal-chalcogenide NCs. First, to achieve the same brightness, the laser power density used to excite a single perovskite NC can be decreased by almost 2 orders of magnitude due to the enhanced absorption cross section. This would greatly reduce the possibility of tissue damage in biolabeling and bioimaging studies, the scattered laser light under resonant or near-resonant excitation conditions, and the working current in electrically driven lightening devices. Second, although the perovskite NCs studied here have a PL peak around ~510 nm, the sizes and compositions can be further manipulated to render broad fluorescent colors spanning the green-to-red wavelength range of traditional metal-chalcogenide NCs. Moreover, the PL peaks of perovskite NCs can be potentially extended to even shorter wavelengths, *e.g.*, with the

$CsPbCl_3$ (ref 32) and $CH_3NH_3PbCl_3$ (ref 33) compositions, for the realizations of blue light-emitting diodes and single photon sources. Third, the fast radiative lifetimes at both room and cryogenic temperatures, together with the suppressed multiphoton emission at high laser power densities, guarantee that single perovskite NCs can be used as a highly efficient, pure single photon source driven at high repetition rates of ~1 GHz.

CONCLUSIONS

To summarize, we have synthesized colloidal $CsPbBr_3$ NCs and successfully demonstrated their capability of emitting single photons. It should be noted that single photon emission was also discovered in single perovskite $CsPbI_3$ NCs in a very recent report,[43] which focused mainly on their PL blinking behavior and multiexciton Auger process. In contrast, we here explore discrepancies between the optical properties of traditional metal-chalcogenide CdSe NCs and the newly synthesized perovskite $CsPbBr_3$ NCs, the latter of which have demonstrated 2 orders of magnitude increase of the absorption cross section and several times decrease of the radiative lifetime. Moreover, the dark-exciton emission commonly encountered in metal-chalcogenide CdSe NCs is almost missing in perovskite $CsPbBr_3$ NCs, signifying a huge difference in the electronic structures of these two types of NC materials. The introduction of perovskite NC optical emitters to the colloidal NC and semiconductor perovskite families will surely stimulate intensive research efforts in future works of material synthesis, fundamental science, and device application. Since perovskite NCs have just come into play in the research community, there is much room for the optimization of the material properties by borrowing nearly two decades of synthesis protocols developed for metal-chalcogenide NCs. For example, proper selection of the passivation ligands and wise adoption of core/shell structures would certainly help to boost the fluorescent quantum efficiency with robust photostability, as well as to suppress or even eliminate the PL blinking and spectral diffusion effects. From the fundamental science point of view, a lot of intriguing issues need to be addressed for single perovskite NCs especially at cryogenic temperatures, including the fine-structure splitting of bright and dark states, as well as the magneto-optical and the coherent properties. Given the fact that the fabrication techniques for solar cells, light-emitting diodes, and photodetectors based on bulk perovskite films have been fully developed, it would also be interesting to see how perovskite NCs behave in these optoelectronic devices.

EXPERIMENTAL SECTION

Synthesis of Colloidal $CsPbBr_3$ NCs. *Chemicals.* Cs_2CO_3 (99.9%) was purchased from J&K. Oleic acid (90%, OA) and octadecene (90%, ODE) were purchased from Alfa Aesar. $PbBr_2$ (99.0%) and oleylamine (80−90%, OLA) were purchased from Aladdin. Toluene (99.5%) was purchased from Beijing Chemical Factory.

Preparation of Cs-Oleate. Cs_2CO_3 (0.8 g), OA (2.5 mL), and ODE (30 mL) were loaded into a 100 mL three-neck flask and dried under vacuum for 1 h at 120 °C. The reaction solution was then kept at 150 °C under N_2 until it became clear.

Synthesis and Purification of $CsPbBr_3$ NCs. ODE (10 mL) and $PbBr_2$ (0.138g) were added into a 50 mL three-neck flask and dried under vacuum for 1 h at 120 °C. Then, dried OLA (1 mL) and dried OA (1 mL) were injected under N_2. After the mixture became clear, the temperature was raised to 180 °C and the Cs-oleate solution (0.8 mL, 0.1 M in ODE, preheated to 100 °C) was quickly injected. The reaction mixture was kept at this temperature for 5 s and then was cooled to room temperature by an ice−water bath. The final NCs were purified by centrifugation and redispersed in toluene to form a long-term colloidally stable solution. The solution absorption and emission measurements were taken with a V-550 UV−visible spectrophotometer from Jasco, and the fluorescent quantum yield was estimated to be ~58%.

Optical Characterizations of $CsPbBr_3$ NCs. One drop of the concentrated or diluted solution of $CsPbBr_3$ NCs was spin-casted onto a fused silica substrate to form a solid film for the optical characterizations of ensemble or single NCs at room temperature. The 405 nm output of a 5 MHz, picosecond diode laser or the 400 nm output of a CW laser was used as the excitation source. The laser beam was focused onto the sample substrate by an immersion-oil objective (NA = 1.4). The PL signal of the ensemble NCs or a single NC was collected by the same objective and sent through a 0.5 m spectrometer to a charge-coupled-device camera for the PL spectral measurements. The PL signal of a single NC can be alternatively sent through a nonpolarizing 50/50 beam splitter to two avalanche photodiodes (APDs) in a time-correlated single photon counting (TCSPC) system with a time resolution of ~250 ps. The TCSPC system was operated under the time-tagged, time-resolved mode so that the arrival times of each photon relative to the laboratory time and the laser pulse time could both be obtained, which allowed us to plot the PL time trajectory and the PL decay curve, respectively. Moreover, the delay times between photons collected by one APD and those by the other could be summed up to yield the second-order autocorrelation $g^{(2)}(\tau)$ functions. For the low-temperature optical characterizations of ensemble or single $CsPbBr_3$ NCs, the sample substrate was contained in a helium-free cryostat operated at ~4 K. Very similar optical setups to those described above were employed except that the immersion-oil objective was replaced by a dry objective (NA = 0.8) and the 485 nm output of a 5.6 MHz, picosecond supercontinuum fiber laser was used as the excitation source.

Calculations of Absorption Cross Sections. The PL saturation curve of either ensemble or single $CsPbBr_3$ NCs can be fitted with a functional form $\propto 1 - e^{-\langle N \rangle} = 1 - e^{-j\sigma}$, where σ and j are the absorption cross section and the laser pump fluence, respectively. The pump fluence j can be calculated from $j = P/FE$, where the laser power density P can be directly measured, F is the laser repetition rate of 5 MHz, and E is the laser photon energy at 405 nm. Based on the above procedures, the absorption cross sections estimated for ensemble $CsPbBr_3$ NCs and a representative $CsPbBr_3$ NC are $\sim 2.33 \times 10^{-13}$ and $\sim 1.23 \times 10^{-13}$ cm^2, respectively. For comparison, commercial Qdot525 colloidal NCs from Invitrogen have a peak emission wavelength of ~525 nm and a molar extinction coefficient ε of 360 000 cm^{-1} M^{-1} at 405 nm. The absorption cross section σ of Qdot525 NCs can be calculated to be $\sim 1.38 \times 10^{-15}$ cm^2 from $\sigma = \ln(10)\ (1000/N_A)\varepsilon$, where N_A is Avogadro's number.

Conflict of Interest: The authors declare no competing financial interest.

Acknowledgment. This work is supported by the National Basic Research Program of China (Nos. 2012CB921801 and 2011CBA00205), the National Natural Science Foundation of China (Nos. 11574147, 91321105, 11274161, and 11321063), Jiangsu Provincial Funds for Distinguished Young Scientists (No. BK20130012), and the PAPD of Jiangsu Higher Education Institutions.

Supporting Information Available: The Supporting Information is available free of charge on the ACS Publications website at DOI: 10.1021/acsnano.5b05769.

Ensemble PL spectra measured at room temperature as a function of the laser excitation power, PL decay curves of single NCs measured at room temperature, PL blinking time trajectories of single NCs, probability densities for the time durations of blinking "on" and "off" periods, $g^{(2)}(\tau)$ measurements of a single NC excited with different pulse laser powers, ensemble PL spectrum measured at cryogenic temperature, and PL decay curves of single NCs measured at cryogenic temperature (PDF)

REFERENCES AND NOTES

1. Kimble, H. J.; Dagenais, M.; Mandel, L. Photon Antibunching in Resonance Fluorescence. *Phys. Rev. Lett.* **1977**, *39*, 691–695.
2. Brunel, C.; Lounis, B.; Tamarat, P.; Orrit, M. Triggered Source of Single Photons Based on Controlled Single Molecule Fluorescence. *Phys. Rev. Lett.* **1999**, *83*, 2722–2725.
3. Lounis, B.; Orrit, M. Single Photon Sources. *Rep. Prog. Phys.* **2005**, *68*, 1129–1179.
4. Shields, A. J. Semiconductor Quantum Light Sources. *Nat. Photonics* **2007**, *1*, 215–223.
5. Michler, P.; Kiraz, A.; Becher, C.; Schoenfeld, W. V.; Petroff, P. M.; Zhang, L.; Hu, E.; Imamoglu, A. A Quantum Dot Single-Photon Turnstile Device. *Science* **2000**, *290*, 2282–2285.
6. Michler, P.; Imamoğlu, A.; Mason, M. D.; Carson, P. J.; Strouse, G. F.; Buratto, S. K. Quantum Correlation among Photons from a Single Quantum Dot at Room Temperature. *Nature* **2000**, *406*, 968–970.
7. Kurtsiefer, C.; Mayer, S.; Zarda, P.; Weinfurter, H. Stable Solid-State Source of Single Photons. *Phys. Rev. Lett.* **2000**, *85*, 290–293.
8. Högele, A.; Galland, C.; Winger, M.; Imamoğlu, A. Photon Antibunching in the Photoluminescence Spectra of a Single Carbon Nanotube. *Phys. Rev. Lett.* **2008**, *100*, 217401.
9. Kolesov, R.; Xia, K.; Reuter, R.; Stohr, R.; Zappe, A.; Meijer, J.; Hemmer, P. R.; Wrachtrup, J. Optical Detection of a Single Rare Earth Ion in a Crystal. *Nat. Commun.* **2012**, *3*, 1029.
10. Castelletto, S.; Johnson, B. C.; Ivady, V.; Stavrias, N.; Umeda, T.; Gali, A.; Ohshima, T. A Silicon Carbide Room-Temperature Single-Photon Source. *Nat. Mater.* **2013**, *13*, 151–156.
11. Perebeinos, V. Two Dimensions and One Photon. *Nat. Nanotechnol.* **2015**, *10*, 485–486.
12. Fernée, M. J.; Tamarat, P.; Lounis, B. Spectroscopy of Single Nanocrystals. *Chem. Soc. Rev.* **2014**, *43*, 1311–1337.
13. Kovalenko, M. V.; Manna, L.; Cabot, A.; Hens, Z.; Talapin, D. V.; Kagan, C. R.; Klimov, V. I.; Rogach, A. L.; Reiss, P.; Milliron, D. J.; et al. Prospects of Nanoscience with Nanocrystals. *ACS Nano* **2015**, *9*, 1012–1057.
14. Kojima, A.; Teshima, K.; Shirai, Y.; Miyasaka, T. Organometal Halide Perovskites as Visible-Light Sensitizers for Photovoltaic Cells. *J. Am. Chem. Soc.* **2009**, *131*, 6050–6051.
15. Lee, M. M.; Teuscher, J.; Miyasaka, T.; Murakami, T. N.; Snaith, H. J. Efficient Hybrid Solar Cells Based on Meso-Superstructured Organometal Halide Perovskites. *Science* **2012**, *338*, 643–647.
16. Kim, H.-S.; Lee, C.-R.; Im, J.-H.; Lee, K.-B.; Moehl, T.; Marchioro, A.; Moon, S.-J.; Humphry-Baker, R.; Yum, J.-H.; Moser, J. E.; et al. Lead Iodide Perovskite Sensitized All-Solid-State Submicron Thin Film Mesoscopic Solar Cell with Efficiency Exceeding 9%. *Sci. Rep.* **2012**, *2*, 591.
17. Chung, I.; Lee, B.; He, J.; Chang, R. P. H.; Kanatzidis, M. G. All-Solid-State Dye-Sensitized Solar Cells with High Efficiency. *Nature* **2012**, *485*, 486–489.
18. Burschka, J.; Pellet, N.; Moon, S.-J.; Humphry-Baker, R.; Gao, P.; Nazeeruddin, M. K.; Grätzel, M. Sequential Deposition as a Route to High-Performance Perovskite-Sensitized Solar Cells. *Nature* **2013**, *499*, 316–319.
19. Zhou, H.; Chen, Q.; Li, G.; Luo, S.; Song, T.-B.; Duan, H.-S.; Hong, Z.; You, J.; Liu, Y.; Yang, Y. Interface Engineering of Highly Efficient Perovskite Solar Cells. *Science* **2014**, *345*, 542–546.
20. Jeon, N. J.; Noh, J. H.; Yang, W. S.; Kim, Y. C.; Ryu, S.; Seo, J.; Seok, S. I. Compositional Engineering of Perovskite Materials for High-Performance Solar Cells. *Nature* **2015**, *517*, 476–480.
21. Tan, Z.-K.; Moghaddam, R. S.; Lai, M. L.; Docampo, P.; Higler, R.; Deschler, F.; Price, M.; Sadhanala, A.; Pazos, L. M.; Credgington, D.; et al. Bright Light-Emitting Diodes Based on Organometal Halide Perovskite. *Nat. Nanotechnol.* **2014**, *9*, 687–692.
22. Xing, G.; Mathews, N.; Lim, S. S.; Yantara, N.; Liu, X.; Sabba, D.; Grätzel, M.; Mhaisalkar, S.; Sum, T. C. Low-Temperature Solution-Processed Wavelength-Tunable Perovskites for Lasing. *Nat. Mater.* **2014**, *13*, 476–480.
23. Dou, L.; Yang, Y.; You, J.; Hong, Z.; Chang, W.-H.; Li, G.; Yang, Y. Solution-Processed Hybrid Perovskite Photodetectors with High Detectivity. *Nat. Commun.* **2014**, *5*, 5404.
24. Manser, J. S.; Kamat, P. V. Band Filling with Free Charge Carriers in Organometal Halide Perovskites. *Nat. Photonics* **2014**, *8*, 737–743.
25. de Quilettes, D. W.; Vorpahl, S. M.; Stranks, S. D.; Nagaoka, H.; Eperon, G. E.; Ziffer, M. E.; Snaith, H. J.; Ginger, D. S. Impact of Microstructure on Local Carrier Lifetime in Perovskite Solar Cells. *Science* **2015**, *348*, 683–686.
26. Shi, D.; Adinolfi, V.; Comin, R.; Yuan, M.; Alarousu, E.; Buin, A.; Chen, Y.; Hoogland, S.; Rothenberger, A.; Katsiev, K.; et al. Low Trap-State Density and Long Carrier Diffusion in Organolead Trihalide Perovskite Single Crystals. *Science* **2015**, *347*, 519–522.
27. Nie, W.; Tsai, H.; Asadpour, R.; Blancon, J.-C.; Neukirch, A. J.; Gupta, G.; Crochet, J. J.; Chhowalla, M.; Tretiak, S.; Alam, M. A.; et al. High-Efficiency Solution-Processed Perovskite Solar Cells with Millimeter-Scale Grains. *Science* **2015**, *347*, 522–525.
28. Dong, Q.; Fang, Y.; Shao, Y.; Mulligan, P.; Qiu, J.; Cao, L.; Huang, J. Electron-Hole Diffusion Lengths > 175 μm in Solution-Grown $CH_3NH_3PbI_3$ Single Crystals. *Science* **2015**, *347*, 967–970.
29. Di, D.; Musselman, K. P.; Li, G.; Sadhanala, A.; Ievskaya, Y.; Song, Q.; Tan, Z.-K.; Lai, M. L.; MacManus-Driscoll, J. L.; Greenham, N. C.; et al. Size-Dependent Photon Emission from Organometal Halide Perovskite Nanocrystals Embedded in an Organic Matrix. *J. Phys. Chem. Lett.* **2015**, *6*, 446–450.
30. Tyagi, P.; Arveson, S. M.; Tisdale, W. A. Colloidal Organohalide Perovskite Nanoplatelets Exhibiting Quantum Confinement. *J. Phys. Chem. Lett.* **2015**, *6*, 1911–1916.
31. Schmidt, L. C.; Pertegas, A.; Gonzalez-Carrero, S.; Malinkiewicz, O.; Agouram, S.; Espallargas, G. M.; Bolink, H. J.; Galian, R. E.; Perez-Prieto, J. Nontemplate Synthesis of $CH_3NH_3PbBr_3$ Perovskite Nanoparticles. *J. Am. Chem. Soc.* **2014**, *136*, 850–853.
32. Protesescu, L.; Yakunin, S.; Bodnarchuk, M. I.; Krieg, F.; Caputo, R.; Hendon, C. H.; Yang, R. X.; Walsh, A.; Kovalenko, M. V. Nanocrystals of Cesium Lead Halide Perovskites ($CsPbX_3$, X = Cl, Br, and I): Novel Optoelectronic Materials Showing Bright Emission with Wide Color Gamut. *Nano Lett.* **2015**, *15*, 3692–3696.
33. Zhang, F.; Zhong, H.; Chen, C.; Wu, X.-G.; Hu, X.; Huang, H.; Han, J.; Zou, B.; Dong, Y. Brightly Luminescent and Color-Tunable Colloidal $CH_3NH_3PbX_3$ (X = Br, I, Cl) Quantum Dots: Potential Alternatives for Display Technology. *ACS Nano* **2015**, *9*, 4533–4542.
34. Stoumpos, C. C.; Malliakas, C. D.; Peters, J. A.; Liu, Z.; Sebastian, M.; Im, J.; Chasapis, T. C.; Wibowo, A. C.;

Chung, D. Y.; Freeman, A. J.; et al. Crystal Growth of the Perovskite Semiconductor $CsPbBr_3$: A New Material for High-Energy Radiation Detection. *Cryst. Growth Des.* **2013**, *13*, 2722–2727.
35. Fang, H.-H.; Raissa, R.; Abdu-Aguye, M.; Adjokatse, S.; Blake, G. R.; Even, J.; Loi, M. A. Photophysics of Organic-Inorganic Hybrid Lead Iodide Perovskite Single Crystals. *Adv. Funct. Mater.* **2015**, *25*, 2378–2385.
36. McGuire, J. A.; Joo, J.; Pietryga, J. M.; Schaller, R. D.; Klimov, V. I. New Aspects of Carrier Multiplication in Semiconductor Nanocrystals. *Acc. Chem. Res.* **2008**, *41*, 1810–1819.
37. Fisher, B.; Caruge, J. M.; Zehnder, D.; Bawendi, M. Room-Temperature Ordered Photon Emission from Multiexciton States in Single CdSe Core-Shell Nanocrystals. *Phys. Rev. Lett.* **2005**, *94*, 087403.
38. Galland, C.; Ghosh, Y.; Steinbruck, A.; Sykora, M.; Hollingsworth, J. A.; Klimov, V. I.; Htoon, H. Two Types of Luminescence Blinking Revealed by Spectroelectrochemistry of Single Quantum Dots. *Nature* **2011**, *479*, 203–207.
39. Klimov, V. I.; Mikhailovsky, A. A.; McBranch, D. W.; Leatherdale, C. A.; Bawendi, M. Quantization of Multiparticle Auger Rates in Semiconductor Quantum Dots. *Science* **2000**, *287*, 1011–1013.
40. Tian, Y.; Merdasa, A.; Peter, M.; Abdellah, M.; Zheng, K.; Ponseca, C. S., Jr.; Pullerits, T.; Yartsev, A.; Sundström, V.; Scheblykin, I. G. Giant Photoluminescence Blinking of Perovskite Nanocrystals Reveals Single-Trap Control of Luminescence. *Nano Lett.* **2015**, *15*, 1603–1608.
41. Wen, X.; Ho-Baillie, A.; Huang, S.; Sheng, R.; Chen, S.; Ko, H.-C.; Green, M. A. Mobile Charge-Induced Fluorescence Intermittency in Methylammonium Lead Bromide Perovskite. *Nano Lett.* **2015**, *15*, 4644–4649.
42. Labeau, O.; Tamarat, P.; Lounis, B. Temperature Dependence of the Luminescence Lifetime of Single CdSe/ZnS Quantum Dots. *Phys. Rev. Lett.* **2003**, *90*, 257404.
43. Park, Y.-S.; Guo, S.; Makarov, N. S.; Klimov, V. I. Room Temperature Single-Photon Emission from Individual Perovskite Quantum Dots. *ACS Nano* **2015**, *9*, 10386.